ASME Journal of Biomechanical Engineering
Online journal at:
https://asmedigitalcollection.asme.org/biomechanical

Kristen LeBar
Department of Mechanical Engineering,
Colorado State University,
Fort Collins, CO 80523

Wenqiang Liu
School of Biomedical Engineering,
Colorado State University,
Fort Collins, CO 80523;
Stanford Cardiovascular Institute,
Stanford University,
Stanford, CA 80523

Adam J. Chicco
Department of Biomedical Sciences,
Colorado State University,
Fort Collins, CO 80523

Zhijie Wang[1]
Department of Mechanical Engineering,
Colorado State University,
Fort Collins, CO 80523;
School of Biomedical Engineering,
Colorado State University,
Fort Collins, CO 80523
e-mail: Zhijie.wang@colostate.edu

Role of Microtubule Network in the Passive Anisotropic Viscoelasticity of Healthy Right Ventricle

Cardiomyocytes are viscoelastic and key determinants of right ventricle (RV) mechanics. Intracellularly, microtubules are found to impact the viscoelasticity of isolated cardiomyocytes or trabeculae; whether they contribute to the tissue-level viscoelasticity is unknown. Our goal was to reveal the role of the microtubule network in the passive anisotropic viscoelasticity of the healthy RV. Equibiaxial stress relaxation tests were conducted in healthy RV free wall (RVFW) under early (6%) and end (15%) diastolic strain levels, and at sub- and physiological stretch rates. The viscoelasticity was assessed at baseline and after the removal of microtubule network. Furthermore, a quasi-linear viscoelastic (QLV) model was applied to delineate the contribution of microtubules to the relaxation behavior of RVFW. After removing the microtubule network, RVFW elasticity and viscosity were reduced at the early diastolic strain level and in both directions. The reduction in elasticity was stronger in the longitudinal direction, whereas the degree of changes in viscosity were equivalent between directions. There was insignificant change in RVFW viscoelasticity at late diastolic strain level. Finally, the modeling showed that the tissue's relaxation strength was reduced by the removal of the microtubule network, but the change was present only at a later time scale. These new findings suggest a critical role of cytoskeleton filaments in RVFW passive mechanics in physiological conditions.
[DOI: 10.1115/1.4064685]

Keywords: myocardial mechanics, myofiber, constitutive modeling, colchicine

1 Introduction

It is widely accepted that the stiffening of the myocardium occurs during heart failure progression and leads to diastolic dysfunction of the ventricle [1]. Recently, correlations between the ex vivo elasticity of the RV free wall and in vivo indices of diastolic function have been reported in small and large animal models [2,3]. Additionally, one study has reported the correlation of the passive elastic properties with systolic function [4]. Thus, the significance of myocardium mechanical behavior in its physiological performance is evident. However, the myocardium is viscoelastic, which means there exist both elastic and viscous resistance during the cyclic deformation in vivo. Viscous resistance originates from the sliding and friction of molecular bonds, and it works as a "damper" to cause a delay between the force and deformation as well as a time-dependent mechanical behavior. The current literature of myocardium biomechanics mainly investigates the tissue as a hyperelastic material and ignores the viscous property. Thus, the understanding of the dynamic mechanical behavior of myocardium remains incomplete.

Increasing evidence of myocardial tissue viscoelasticity in both left and right ventricles (LV, RV) has been reported recently, including those from our group [5–9]. The myocardium is a complex tissue comprising of myofibers, collagen, vasculature, and other extracellular matrix (ECM) components, which all exhibit viscoelastic behavior and contribute to the anisotropic mechanical properties of the tissue. It has long been established that cardiomyocytes (CM) or papillary muscles exhibit viscoelastic properties [10–15]. CM (myofibers) are responsible for the contractile function of the organ and the contractility is dependent on the viscoelastic behavior of the cell [12,16,17]. In a study of adult CM from healthy feline RV, it was revealed that the depolymerization of microtubules (MT) via colchicine treatment reduced CM viscoelasticity and enhanced the extent and velocity of shortening [18], demonstrating a critical role of the MT network in CM mechanics and contractile function. Additionally, Caporizzo et al. found that the treatment of colchicine on isolated CM from healthy and failing LVs leads to a reduction of the cell viscoelasticity (viscosity and elasticity) [10–12,16]. They obtained both stress relaxation and hysteresis mechanical data of the CM, but the mechanical characterization was for one-dimensional mechanics of the isolated muscle cells. Thus, the role of the MT network in tissue-level biaxial mechanics of the myocardium remains largely unknown [14].

[1]Corresponding author.
Manuscript received October 19, 2023; final manuscript received January 30, 2024; published online March 19, 2024. Assoc. Editor: Kristin S. Miller.

Therefore, the aim of this study is to investigate the contributions of MT network to the passive anisotropic viscoelasticity of healthy RVs. We conducted equibiaxial stress relaxation in healthy rat RVFW with and without colchicine treatment to remove MT polymerization. We then applied a Fung-type QLV model to the experimental data to further characterize the relaxation behavior of the RVFW. Our study revealed that (1) RVFW viscosity, not elasticity, was increased from subphysiological to physiological stretch rate in both directions; (2) the RVFW elasticity and viscosity was enhanced from early to late diastolic strain levels in both directions; (3) the removal of MT network reduces RVFW elasticity and viscosity at early diastolic strain only, with a stronger degree of reduction in elasticity in the longitudinal direction; (4) from the QLV modeling, the contribution of the MT network to the relaxation strength is the strongest in the late (G_3) rather than early (G_1 and G_2) relaxation time constants. To our knowledge, this is the first tissue-level examination of the MT's role in the RVFW anisotropic viscoelasticity. These findings will deepen the understanding of the microstructural contributions to RV mechanics.

2 Materials and Methods

2.1 Ex Vivo Equibiaxial Mechanical Testing. All animal procedures were approved by and performed in accordance with the Institutional Animal Care and Use Committees (IACUC, protocol #1438) at Colorado State University. 9-week-old healthy adult male Sprague-Dawley rats (body weight ~360 g) (n ¼ 8) were euthanized by CO_2 inhalation, and the heart was excised and placed in phosphate buffer solution (PBS) on ice. The RVFW was dissected in cardioplegic solution and placed in 30-mM 2,3-butanedione monoxime solution at body temperature (37 °C) for 30 min to remove the active contractility of the myocardium. The outflow tract direction was defined as the longitudinal (L) direction. The tissue was then preloaded to approximately 0.05 N to specify the zero-stress configuration, and calipers were used to measure the thickness of the square sample. 15 cycles of equibiaxial preconditioning were then conducted (at 1 Hz and 20% maximal strain).

Right ventricle tissue then underwent equibiaxial stress relaxation to obtain the passive, biaxial viscoelastic behavior, using an in-house biaxial tester [19]. It is known that the myofibers are dominant in myocardial mechanics at low (early diastole) strain levels while collagen fibers dominate the mechanical behavior at high (late diastole) strain levels [2,20]. Thus, the RV was stretched to a strain of 6% and 15%, which corresponds to early and late diastolic strain, respectively. For each strain level, the tissue was tested at two stretch rates (ramp speeds) that correspond to a subphysiological (1 Hz) and physiological (5 Hz) heart rate of the adult rat, respectively. Between each test, a resting time of 10 times that of the previous testing period was included to ensure the full recovery of the tissue. After the tissue was tested at the baseline condition (base), 0.3 mM colchicine (COL) (Sigma-Aldrich) was added to the perfusate for 30 min to depolymerize the MT in the RVFW, and the same mechanical testing was performed. The removal of the MT network was confirmed by a notable (30%) reduction in the peak force during stress relaxation test.

2.2 Data Analysis. After data collection, the engineering (r) and the second Piola–Kirchhoff (P–K) (S) stresses, and Green strain (E) were calculated for each direction (r ¼ F=A_0, S ¼ r=k_i, and E ¼ $\frac{1}{2}$ðk$_i^2$ − 1Þ, where F is the measured force, A_0 is the initial cross-sectional area, and k_i is the stretch in the i ¼ L, C direction with L and C denoting the longitudinal and circumferential directions, respectively.

Relaxation modulus (relax modulus) from each direction was used as a measure of RVFW elasticity and was calculated as described previously [8]. We further quantified RV elasticity and viscosity from the stress relaxation raw data by the stored energy (W_S) and dissipated energy (W_d), respectively, using the 2nd P–K stress formulation. At any input strain level (e_{input}), we derived W_S as a function of time (t) using the total area (A_S) under the curve from

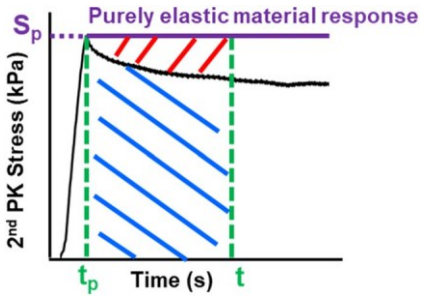

Fig. 1 The stored energy (W_S) and dissipated energy (W_d) are derived from the blue (A_S) and red (A_d) shaded area, respectively. These integrated areas (A_S and A_d) are calculated between the time (t_p) of peak stress (S_p) and any time point (t) during relaxation.

peak stress to the relaxed stress at any time (t) (Eq. (1)), and derived W_d using the area (A_d) between the stress relaxation curve and the curve describing the response of a purely elastic material from peak stress to the relaxed stress at time t (Eq. (2)) and (Fig. 1)

$$W_S(t) = \int_{t_p}^{t} S(t)\, e_{input}\, dt = e_{input} \int_{t_p}^{t} S(t)\, dt = e_{input} \times A_S \quad (1)$$

$$W_d(t) = \int_{t_p} S_p e_{input}\, dt - \int_{t_p}^{t} S(t)\, e_{input}\, dt = e_{input} \left[\int_{t_p}^{t} S_p\, dt - \int_{t_p}^{t} S(t)\, dt \right] = e_{input} \times A_d \quad (2)$$

2.3 Microstructural Measurements. The tested RV tissue samples were fixed in 10% formalin and embedded in paraffin wax. The longitudinal (outflow tract) direction was marked. The tissue blocks were sectioned into eight serial slides from the epi- to endocardial side and stained with Picrosirius Red for fiber orientation measurement using in-house MATLAB codes [5]. Briefly, the transmural fiber change was quantified from the serial histology sections as described previously [21]. Each serial section was imaged using bright field light microscopy and the main collagen fiber direction in the plane was calculated using an orientation distribution function. The transmural fiber orientation was then represented by a Beta distribution function to fit a surface to the three-dimensional data. The mean transmural fiber orientations were calculated using a one-dimensional Hermit shape function and used as the main fiber orientation in the model fitting.

2.4 Constitutive Model of Tissue Viscoelasticity: Quasi-Linear Viscoelastic Fitting. An established QLV model was used to fit the experimental data as previously described [5]. Assuming incompressibility and negligible shear deformation, the QLV construction for the 2nd Piola–Kirchhoff (PK) stress tensor (S) can be presented as [22]

$$S(E,t) = S_0 + \int_0^t G(t-s) : \frac{\partial S^e}{\partial E} : \frac{\partial E(s)}{\partial s}\, ds \quad (3)$$

where E is the Green strain tensor, t is time, S_0 is the initial stress pretension obtained from the force in the zero stress configuration, which was set to zero [22–24], G(t) is the reduced relaxation function, S^e is the instantaneous elastic stress, and s is a time variable of integration. The strain tensor (E) was prescribed by the global position of the actuators, with linear increments during the ramp period and held fixed during the relaxation period. Only normal (longitudinal and circumferential) strains were applied, and shear strains were negligible at the boundaries at all times. The anisotropic Ogden strain energy density function (w) was used to derive the instantaneous elastic stress S^e [24,25]

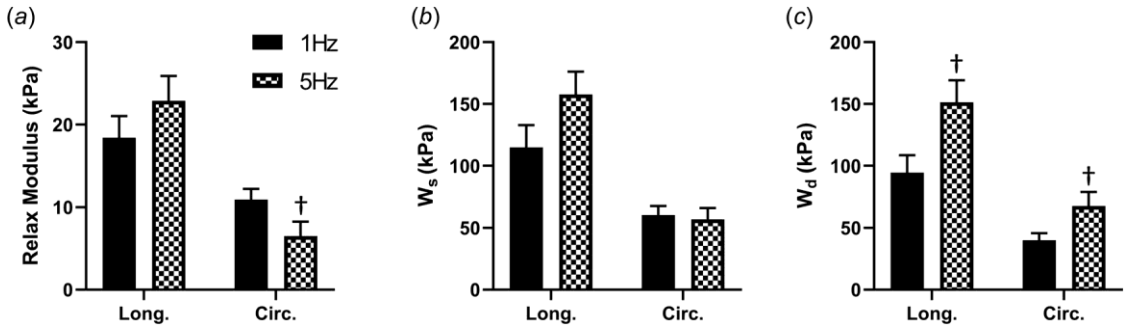

Fig. 2 RV elasticity (*a*) and (*b*) and viscosity (*c*) at subphysiological (1 Hz) and physiological stretch rates (5 Hz). y$p < 0.05$ compared to 1 Hz in same direction.

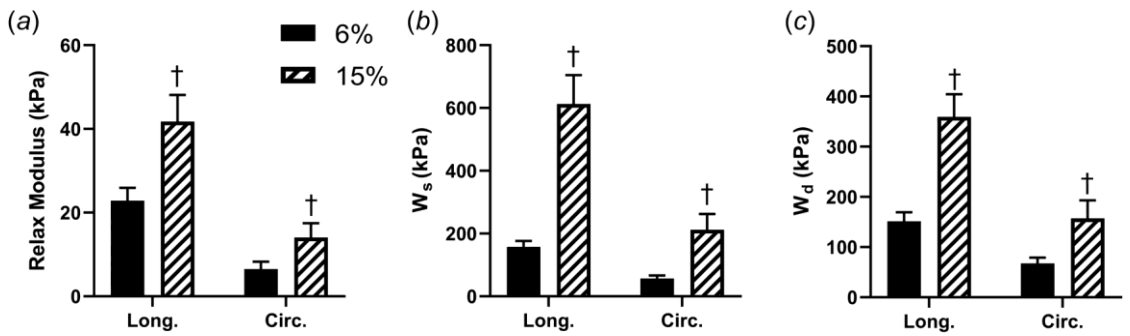

Fig. 3 RV elasticity (*a*) and (*b*) and viscosity (*c*) at early (6%) and late (15%) diastolic strain levels. y$p < 0.05$ compared to 6% in same direction.

$$w = \frac{2l}{a^2}\left[k^a_1 + k^a_2 + k^a_3 - 3\right] + \frac{2kl}{a^2}\left[I_4^{\frac{a}{2}} + I_4^{-\frac{a}{2}} - 3\right] \tag{4}$$

using

$$S^e = 2\frac{dw}{dC} - pC^{-1} \tag{5}$$

where the parameters a, l, and k represent the nonlinearity, infinitesimal shear modulus and anisotropy of the tissue, respectively. The principal stretch k_i are the diagonal elements of the deformation gradient tensor when no shearing is present. C is the right Cauchy-Green deformation tensor and C = 2E + I. With the L and C directions aligned to the k_L and k_C, respectively, the anisotropic invariant I_4 was equal to

$$I_4 = a_0 \cdot Ca_0 = k^2_L\cos^2\theta + k^2_C\sin^2\theta \tag{6}$$

where a_0 is a vector describing the fiber orientation defined by the θ, and $\theta = 0$ represents the fiber aligned along the longitudinal (outflow tract) direction.

In this study, the reduced relaxation function $G(t)$ in each direction was defined by the Prony series as

$$G(t) = G_1 + \sum_{n=1}^{3} G_n e^{-t/\tau_n} \tag{7}$$

such that

$$G_1 + G_2 + G_3 + G_1 = 1 \tag{8}$$

where G_1 is the long-term relaxation coefficient, which quantifies the proportion of instantaneous elastic stress S^e remaining in the RVFW over a long (infinite) period. G_n are relaxation coefficients corresponding to the following time constants in the relaxation: $\tau_1 = 0.3$ s, $\tau_2 = 3$ s, and $\tau_3 = 30$ s. These time constants were selected because they have been shown to successfully fit ovine RVFW viscoelastic behavior. Each G_n represents the relaxation strength at the corresponding time constant.

2.5 Statistical Analysis. Paired student t-test was used to compare experimental data between stretch rates, strain levels, and directions, as well as computational results. Two-way ANOVA with Tukey posthoc test was performed to compare viscoelastic properties before and after MT depolymerization and between directions. The statistical analyses were performed using Graphpad Prism version 10.1. All data are presented as mean±SEM. $p < 0.05$ was considered statistically significant.

3 Results

3.1 Right Ventricle Free Wall Viscosity, Not Elasticity, Is Elevated From Sub-Physiological to Physiological Ramp Speed in Both Directions. We first examined the effect of ramp speed on RV viscoelasticity in the baseline condition. RV relaxation modulus was reduced from subphysiological to physiological ramp speeds in the C direction only (Fig. 2(*a*)), and RV stored energy was not affected significantly by ramp speed (Fig. 2(*b*)). These results showed that a higher ramp speed does not enhance RV elasticity. However, RV viscosity was markedly elevated with increasing ramp speed in both directions, as evidenced by the dissipated energy (Fig. 2(*c*)). Therefore, RVFW viscosity, not elasticity, was elevated from subphysiological to physiological ramp speeds.

3.2 Enhanced Right Ventricle Free Wall Elasticity and Viscosity in Both Directions From Early to Late Diastole Strain. We also investigated the strain dependency of RV viscoelasticity in the baseline condition. We observed significant elevation in relaxation modulus with the increased strain in both directions (Fig. 3(*a*)). Additionally, the stored energy was higher at

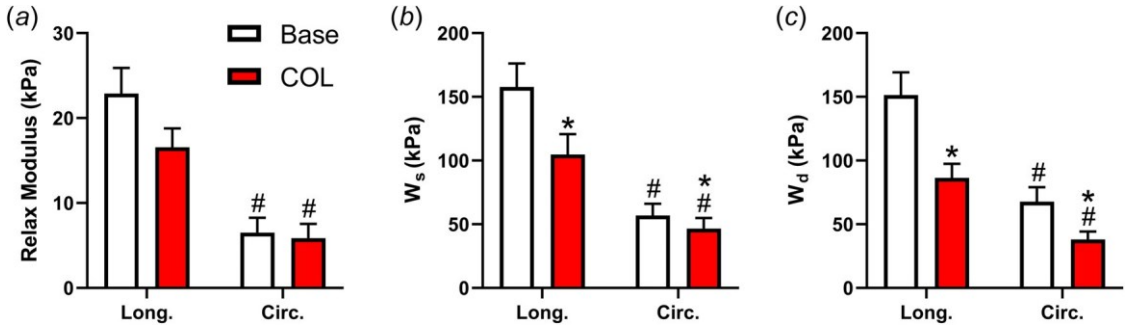

Fig. 4 RV elasticity (*a*) and (*b*) and viscosity (*c*) after the removal of the MT network (COL) under 6% strain and ramp speed corresponding to 5 Hz. *$p < 0.05$ compared to baseline in same direction; #$p < 0.05$ compared to L direction in same condition.

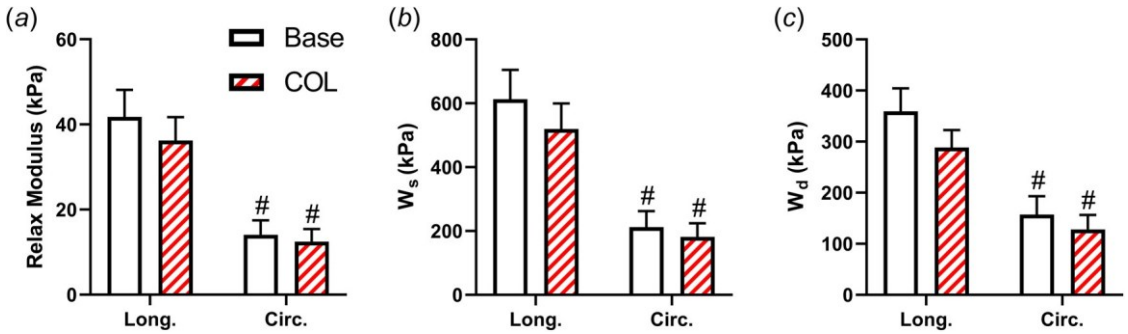

Fig. 5 RV elasticity (*a*) and (*b*) and viscosity (*c*) after the removal of the MT network (COL) under 15% strain and ramp speed corresponding to 5 Hz. *$p < 0.05$ compared to baseline in same direction; # $p < 0.05$ compared to L direction in same condition.

15% strain compared to 6% in both directions, too (Fig. 3(*b*)). Therefore, a strain-stiffening behavior was observed in the RV in both directions. We then observed an elevated RV viscosity with the increased strain, revealed by increased dissipated energy from the early to late diastole strain (Fig. 3(*c*)).

3.3 Removal of Microtubules Network Weakens Right Ventricle Free Wall Elasticity and Viscosity at Early and Late Diastole Strains. Next, we examined the role of the MT network at the physiological ramp speed and first at 6% strain to represent early diastolic mechanical behavior. We observed negligible effect of colchicine on relaxation modulus. However, the tissue's stored energy was reduced in both directions, with a larger percentage of decrease in the L direction (Fig. 4(*b*)). These results indicate that the MT contributes to RV elasticity in both directions and with a stronger effect in the L direction. The responses of RV dissipated energy to colchicine treatment displayed similar behavior as observed in the stored energy (Fig. 4(*c*)), but the percentage of reduction in dissipated energy was similar between directions. These results suggest an equivalent contribution of the MT to tissue viscosity at both directions.

Next, we examined the contribution of the MT network at a higher strain (15%) to capture the late diastolic mechanical behavior. We observed different findings at 15% strain than at 6% strain, with no significant effect of colchicine in elasticity or viscosity (Fig. 5). These results indicate a nonsignificant contribution of MT to RV viscoelasticity at higher strains. However, the anisotropy in all parameters was maintained after the removal of the colchicine treatment, suggesting a weakened MT network does not impact fiber alignment.

3.4 Quasi-Linear Viscoelastic Modeling Shows Stretch Rate-Dependent Changes in Right Ventricle Free Wall Viscoelasticity. We next applied a QLV formulation to the experimental data at 6% of strain since a stronger effect of MT was noted at early diastolic strains. We found that the shear modulus was elevated from subphysiological to physiological ramp speed, indicating a greater resistance to shear deformation at elevated stretch rates (Fig. 6(*a*)). We did not observe significant difference in anisotropy index (β) between the stretch rates (Fig. 6(*b*)). The elastic anisotropy value was negative at both stretch rates, indicating a stiffer mechanical behavior in the cross-fiber (*C*) direction. Finally, we examined the average relaxation function ($G(t)$) of the RV tissue. At the subphysiological ramp speed, the $G(t)$ curve in *L* direction was above that in the *C* direction; but at the physiological ramp speed, the $G(t)$ curve in the *C* direction was above that in the *L* direction (Fig. 6(*c*)). These data indicate a change in the viscous anisotropy with increasing stretch rate. Moreover, the 5-Hz curves are higher than the 1-Hz curves, suggesting a stronger viscous relaxation at a physiological stretch rate.

3.5 Quasi-Linear Viscoelastic Modeling Shows Strain Dependent Changes in Right Ventricle Free Wall Viscoelasticity. We then compared the modeling parameters between 6% and 15% strain levels obtained at the physiological stretch rate. First, there was a significant increase in shear modulus from 6% to 15% of strain (Fig. 7(*a*)). The elastic anisotropy was not significantly impacted by strain levels (Fig. 7(*b*)). Interestingly, though, from the average relaxation function, $G(t)$, we observed that the curves at 15% strain were lower than the curves at 6% strain in both directions (Fig. 7(*c*)).

3.6 Microtubules Network Contributes to Right Ventricle Free Wall Relaxation Strength Predominantly at a Later Time Scale (G_3) and in the Longitudinal Direction. Finally, RV relaxation strength (G_n) and the overall relaxation behavior ($G(t)$) were compared before and after the removal of MT under physiological stretch rates. At the early diastolic strain (6%), we observed a reduced relaxation strength at a later time constant (G_3) and in the *L* direction only after MT removal (Figs. 8(*a*) and 8(*b*)). Additionally, the average reduced relaxation function curves were lower after MT removal, and the reduction was more pronounced in

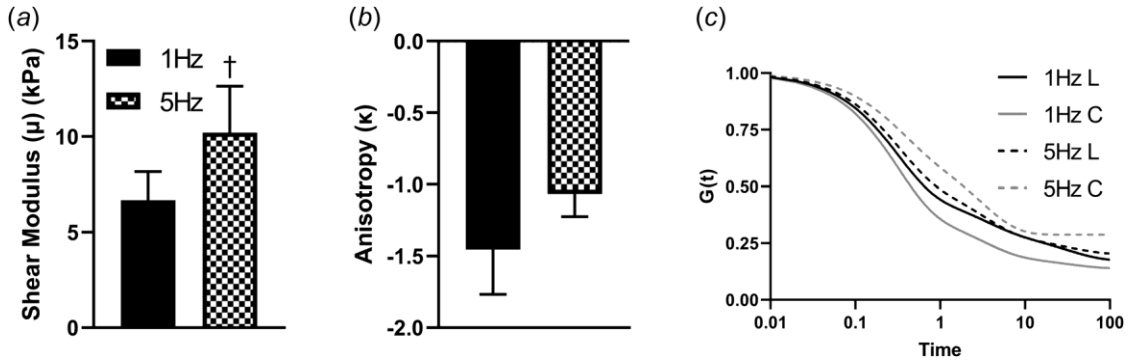

Fig. 6 RV elasticity (*a*), elastic anisotropy (*b*), and average relaxation function G(t) (*c*) at subphysiological (1 Hz) and physiological (5 Hz) stretch rates derived from the QLV modeling. y $p < 0.05$ compared to 1 Hz.

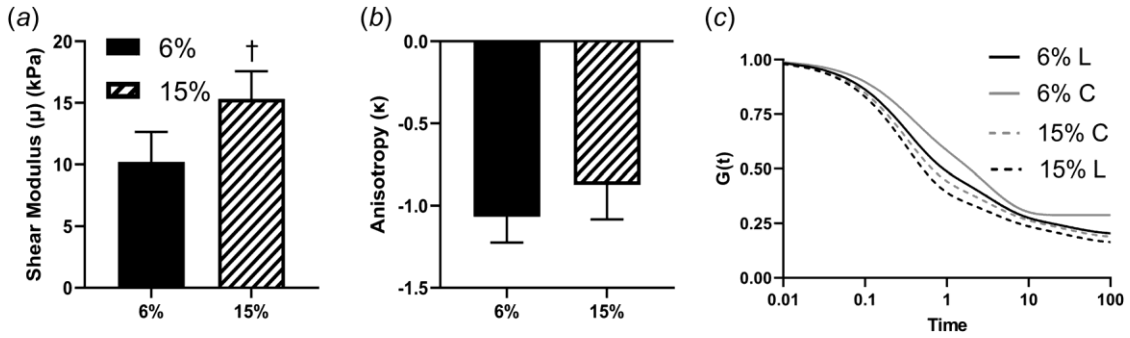

Fig. 7 RV elasticity (*a*), anisotropy (*b*), and average relaxation function *G*(*t*) (*c*) at early diastolic (6%) and late diastolic (15%) strain levels from the QLV modeling. y $p < 0.05$ compared to 6%.

the *C* direction (Fig. 8(*c*)). At the late diastolic strain (15%), we observed a similar effect of MT removal on the relaxation strength (Figs. 8(*d*)–8(*f*)). However, the reduction in G_3 at the 15% strain level (8%) was less than that at the 6% strain level (23%), indicating a stronger effect of the MT network at the early diastolic strain level compared to the late diastolic strain level. Similarly, after the removal of the MT network, the average reduced relaxation function (G(t)) curve was shifted down from the baseline curve, and the shift was more pronounced at the 6% strain level than at the 15% strain level (Figs. 8(*c*) and 8(*f*)).

4 Discussion

To our knowledge, this is the first investigation of the effect of MT network on healthy RVFW anisotropic viscoelasticity. We originally found that (1) higher (physiological) stretch rate elevates RV viscosity in both directions as well as the shear modulus; (2) higher (end diastolic) strain enhances RV elasticity and viscosity in both directions; (3) the removal of MT network reduces RV elasticity and viscosity in both directions but at the end diastolic strain level only, with a larger degree of reduction in elasticity in the longitudinal direction; (4) QLV modeling revealed that the MT network plays a dominant role in a later relaxation time constant (G_3) and its effect on tissue viscoelasticity is stronger at early than late diastolic strain. The understanding of contributions of MT network to RV tissue-level mechanics further deepens the knowledge of RV dynamic mechanical behavior regulated by cytoskeleton components.

4.1 Stretch Rate-Dependent Changes in Right Ventricle Free Wall Viscosity and Elasticity.

The mechanical behavior of tissues, including their viscoelasticity, can be strain or stretch rate dependent [26]. For instance, the conduit arteries (systemic or pulmonary) exhibit frequency-dependent viscoelastic behavior when tested under cyclic deformations [27–29]. Interestingly, while healthy pulmonary artery had increased elasticity (dynamic elastic modulus) as frequency increases, the hypertensive pulmonary artery had decreased elasticity [29]. Recently, stretch rate-dependent change in elasticity was also reported in heart valves. Anssari-Benam et al. reported elevated elastic modulus in semilunar valves from quasi-static to dynamic loadings [30,31]. Stretch rate-dependent viscoelasticity of myocardium has been reported as well [6,9,32]. At the cellular level, Caporizzo et al. found that the isolated cardiomyocytes display greater dissipation of energy and elastic modulus under diastolic stretch speed (10% over 5 ms) compared to subphysiological stretch speed (10% over 200 ms) [16]. But at the tissue-level measurements, discrepant results are observed. Sommer et al. investigated the mechanical behavior of human LV and RV free walls and showed that the hysteresis loop area (i.e., viscosity) enlarges from quasi-static (3 mm/min) to dynamic (30 mm/min) stretch rates [9], but the slope of the loop (i.e., elasticity) was not affected significantly. We observed similar responses in rat RVs here: with elevated strain rate (from subphysiological to physiological), the RV viscosity was strengthened in both directions (Figs. 2(*c*) and 6(*c*)). However, the increase in relaxation modulus or stored energy (W_S) was lacking (Figs. 2(*a*) and 2(*b*)). These findings suggest that different molecular mechanisms may be responsible for myocardium tissue viscosity and elasticity, and these two mechanical properties may be independent.

Furthermore, our results from model fitting showed that RV shear modulus was increased from low to high ramp speeds (Fig. 6(*a*)) [7,16]. For isotropic linear elastic materials, the shear modulus and elastic modulus are interdependent, and the changes in these parameters are in parallel. But in anisotropic materials, elastic modulus is direction-dependent, while shear modulus is direction-independent; thus, the two moduli will not necessarily have similar alterations under different loads. Moreover, the shear modulus measures the intrinsic resistance to *shear* deformation and the elastic

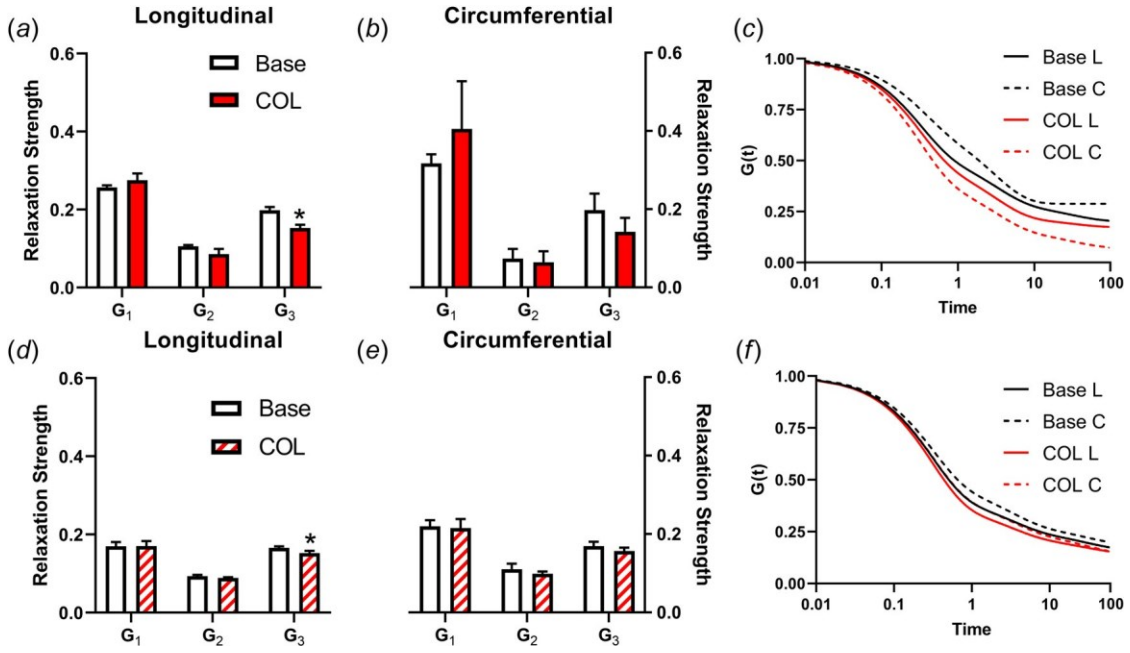

Fig. 8 RV relaxation strength (Gn) (*a*) and (*b*), (*d*) and (*e*) and reduced relaxation function, $G(t)$ (*c*) and (*f*), before and after the removal of the MT network (COL) measured under early (*a*)–(*c*) and late (*d*)–(*f*) diastolic strains at physiological stretch rate in each direction. $^*p < 0.05$ compared to baseline in same direction.

modulus measures the intrinsic resistance to *tensile* deformation. In our experiment protocol, the shear deformation of the tissue was negligible. But the modeling result suggests that the shear elastic resistance is elevated at higher heart rates during the in vivo three-dimensional deformation of the heart wall. The physiological significance awaits further investigations. Finally, we used an Ogden strain energy function to characterize the elastic response in the QLV modeling because the same model has been shown to successfully describe the viscoelastic behavior of RVFW [5]. Future studies can explore other commonly used hyperelastic models to predict the elastic/Young's modulus of the tissue. Overall, our results clearly show the importance of using a physiological stretch rate in capturing the viscous and elastic behavior of myocardium tissue.

4.2 Strain-Dependent Changes in Right Ventricle Free Wall Elasticity and Viscosity. Strain-stiffening phenomena has been found in a variety of biological tissues, and a typical experimental measurement of it is through the J-shaped stress–strain curve. For myocardium tissues, numerous studies have reported this nonlinear behavior of the tissue [5,9,14,33], with a low elastic modulus at small strains and high elastic modulus at high strains. Similar behavior can be found at the cellular level of myocardium as well [11]. Strain-stiffening phenomena has been explained by the increased alignment or recruitment of stiffer (collagen) fibers or by the increased crosslinks between the polymers as the strain increases. As expected, we observed a larger relaxation modulus and stored energy (W_S) of the RV at late diastolic strains (Figs. 3(*a*) and 3(*b*)). Results from the QLV modeling showed a similar trend in shear modulus (Fig. 7(*a*)). Thus, our results are consistent with findings from prior work. Moreover, our study has found novel strain-dependent viscous behavior in the RV: the measurement of W_d showed significant elevation in RV viscosity from early to end diastole strains. However, the average reduced relaxation function ($G(t)$) curves were reduced at larger strains in both directions (Fig. 7(*c*)), indicating a weakened viscous behavior. In most of our data, the measurements of W_d and $G(t)$ give consistent findings as we treat those parameters as indicators of viscosity. However, the discrepancy here calls for a deeper reflection of the measurements of viscosity through these parameters. In the present study, W_d is essentially a measure of the total dissipated energy during the relaxation phase, and it is affected by both the intrinsic viscous property as well as the peak stress, which involves the elastic property of the material. However, the $G(t)$ is a modeling result that is derived after the separation of the elastic and viscous stresses, so it is not affected by the elastic property of the material. It can be viewed as a representation of the intrinsic viscous property. Thus, although both parameters can capture the viscous behavior of the material, the W_d is more of a measure of the extrinsic viscosity, where the relaxation strength (G_n) is a modeling metric of the intrinsic viscosity.

4.3 Removal of the Microtubules Network Reduces Right Ventricle Free Wall Viscosity and Elasticity in a Strain-Dependent and Direction-Dependent Manner. As the first investigation on the role of MT in RVFW tissue viscoelasticity, we found that RV elasticity and viscosity were significantly reduced after the removal of MT network in both directions and at early diastolic strain level only (Fig. 4). The responses of isolated cardiomyocytes to MT removal display similar behavior, with both cell elasticity and viscosity reduced [12,15,16,18,34]. Therefore, our and prior findings have confirmed a critical contribution of MT network to the myocardium viscoelasticity at tissue and cell level, respectively. However, there are some new findings from this current work.

First, we found that the reduction in RV viscoelasticity after the removal of MT network was significant at the early diastolic strain (6%) but not at the late diastolic strain (15%). The strain-dependent effect of MT network shows a larger effect of MT at small strains, and this could be explained with the increasing recruitment of collagen at large strains. It is known that at early diastole, myofibers play a more dominant role in myocardial mechanics; while at late diastole, collagen has been fully recruited and is contributing more to the mechanical behavior of the tissue [2], resulting in higher elasticity at elevated strains [5]. Second, the effect of MT network on elasticity and viscosity is different and can be direction dependent. At early diastolic strain, we observed a stronger reduction in RV elasticity in the L direction compared to the C direction (~37% versus 18%). However, the reduction in viscosity between the two directions was nearly identical (~44%). The different changes of

reduction in elasticity and viscosity suggest that MT network contributes to these mechanical behaviors distinctly. The MT cytoskeletons are predominantly aligned in the main direction of contraction in the muscle cells [11]. Thus, our results indicate that the MT contributes to RV viscosity regardless of preferred direction, whereas its contribution to RV elasticity is more dependent on the alignment. Various molecular mechanisms may be responsible for the elasticity and viscosity of MT network. Titin, a sarcomeric protein, is interconnected with the MT network and provides structural support to the network. Disruption of the MT network, as in after depolymerization, may affect the mechanical behavior of titin, and we acknowledge its potential role in myocardial mechanics.

4.4 Microtubules Network Contributes to the Relaxation Behavior of Right Ventricle Free Wall at a Later Time Scale, With a Stronger Effect at the Early Diastolic Strain Level. Despite the novel findings from the experimental work, the computational work done in this study provides further insights on the relaxation behavior of the tissue that experimental data cannot provide. In this study, we used three terms of G_n to capture the relaxation strength of the RV at the beginning of relaxation and the G_{inf} to capture the relaxation strength at the end (equilibrium) of the relaxation.

The removal of the MT network at both strain levels resulted in a reduction of relaxation strength at 30 s. after peak stress (i.e., s_{30}) (Fig. 8). This change was only present in the L direction. Interestingly, there were no significant effects of the MT network on G_n at early relaxation times. Our results suggest that the MT is playing a dominant role in the relaxation response at a later time scale. In this traditional Fung's QLV model, G_n mainly describes the relaxation strength at different time constants of the relaxation. Whether it is related to different biological components (e.g., myofiber or collagen) or different molecular structures (e.g., tiny fibrils or large fibers) remains unknown. Nordsletten et al. have proposed that the hierarchical structure of the extracellular matrix is responsible for the molecular mechanism of relaxation at different time scales—from fibrils, to fibers, to bundles, to sheets—in human myocardium [35]. If this is the case, our results suggest that the MT network serves as an intermediate fibrous component, and other smaller components (e.g., actin, collagen fibril) may be responsible for more earlier relaxation responses. MT network not only contains cytoskeletons with the diameter of ~ 25 nm but also has crosslinks between the coiled polymers. How the microstructure of crosslinks (in L and C directions) is involved in the relaxation strength distribution is unknown. Moreover, there are influences from other intracellular and extra-cellular components as well as the interactions between these components. Therefore, future work should investigate how the relaxation constants are affected by various biological elements and the architectures in a complex tissue like myocardium.

5 Conclusions

This is the first study to investigate the contribution of microtubules to the RVFW anisotropic viscoelasticity. Our results showed that the RV exhibits stretch rate-dependent and strain-dependent viscoelastic behavior. The removal of MT network reduces RV viscosity and elasticity in both directions, with a significant reduction at early but not late diastolic strain and a larger decrease in elasticity in the longitudinal direction. From the QLV modeling, it is shown that the MT network plays a dominant role in a later relaxation time constant and the effect of MT on tissue relaxation is stronger at early than late diastolic strain. These new findings characterize the distinct role of the MT network in healthy RVFW passive anisotropic viscoelasticity. Such knowledge will deepen the understanding of the microstructural contributions to myocardial mechanics.

Funding Data

- National Science Foundation (NSF) (Grant No. 2244994; Funder ID: 10.13039/100000001).

Data Availability Statement

The datasets generated and supporting the findings of this article are obtainable from the corresponding author upon reasonable request.

References

[1] Liu, W., and Wang, Z., 2019, "Current Understanding of the Biomechanics of Ventricular Tissues in Heart Failure," Bioengineering, 7(1), p. 2.
[2] Jang, S., Vanderpool, R., Avazmohammadi, R., Lapshin, E., Bachman, T., Sacks, M., and Simon, M., 2017, "Biomechanical and Hemodynamic Measures of Right Ventricular Diastolic Function: Translating Tissue Biomechanics to Clinical Relevance," J. Am. Heart Assoc., 6(9), p. e006084.
[3] Liu, W., Nguyen-Truong, M., Labus, K. M., Boon, J., Easley, J., Monnet, E., Puttlitz, C. M., and Wang, Z., 2020, "Correlations Between the Right Ventricular Passive Elasticity and Organ Function in Adult Ovine," J. Integr Cardiol., 6(3), pp. 1–6.
[4] Borlaug, B. A., Redfield, M. M., Melenovsky, V., Kane, G. C., Karon, B. L., Jacobsen, S. J., and Rodeheffer, R. J., 2013, "Longitudinal Changes in Left Ventricular Stiffness: A Community-Based Study," Circ. Heart Failure, 6(5), pp. 944–952.
[5] Liu, W., Labus, K. M., Ahern, M., LeBar, K., Avazmohammadi, R., Puttlitz, C. M., and Wang, Z., 2022, "Strain-Dependent Stress Relaxation Behavior of Healthy Right Ventricular Free Wall," Acta Biomater., 152, pp. 290–299.
[6] Ahmad, F., Liao, J., Soe, S., Jones, M. D., Miller, J., Berthelson, P., Enge, D., et al., 2018, "Biomechanical Properties and Microstructure of Neonatal Porcine Ventricles," J. Mech. Behav. Biomed. Mater., 88, pp. 18–28.
[7] Demer, L. L., and Yin, F. C., 1983, "Passive Biaxial Mechanical Properties of Isolated Canine Myocardium," J. Physiol., 339, pp. 615–630.
[8] Liu, W., Nguyen-Truong, M., Ahern, M., Labus, K. M., Puttlitz, C. M., and Wang, Z., 2021, "Different Passive Viscoelastic Properties Between the Left and Right Ventricles in Healthy Adult Ovine," ASME J. Biomech. Eng., 143(12), p. 121002.
[9] Sommer, G., Schriefl, A., Andra, M., Sacherer, M., Viertler, C., Wolinski, H., and Holzapfel, G., 2015, "Biomechanical Properties and Microstructure of Human Ventricular Myocardium," Acta Biomater., 24, pp. 172–192.
[10] Caporizzo, M. A., and Prosser, B. L., 2021, "Need for Speed: The Importance of Physiological Strain Rates in Determining Myocardial Stiffness," Front. Physiol., 12, p. 696694.
[11] Caporizzo, M. A., and Prosser, B. L., Jun. 2022, "The Microtubule Cytoskeleton in Cardiac Mechanics and Heart Failure," Nat. Rev. Cardiol., 19(6), pp. 364–378.
[12] Caporizzo, M. A., Chen, C. Y., Salomon, A. K., Margulies, K. B., and Prosser, B. L., 2018, "Microtubules Provide a Viscoelastic Resistance to Myocyte Motion," Biophys. J., 115(9), pp. 1796–1807.
[13] Stroud, J. D., Baicu, C. F., Barnes, M. A., Spinale, F. G., and Zile, M. R., 2002, "Viscoelastic Properties of Pressure Overload Hypertrophied Myocardium: Effect of Serine Protease Treatment," Am. J. Physiol. Heart Circ. Physiol., 282(6), pp. H2324–H2335.
[14] Harris, T. S., Baicu, C., Conrad, C., Koide, M., Michael, B. J., Barnes, M., Cooper, G., IV, and Zile, M. R., 2002, "Constitutive Properties of Hypertrophied Myocardium: Cellular Contribution to Changes in Myocardial Stiffness," Am. J. Physiol. Heart Circ. Physiol., 282(6), pp. H2173–H2182.
[15] Zile, M. R., Koide, M., Sato, H., Ishiguro, Y., Conrad, C., Michael, B. J., Morgan, J., and Cooper, G., IV, 1999, "Role of Microtubules in the Contractile Dysfunction of Hypertrophied Myocardium," J. Am. Coll. Cardiol., 33(1), pp. 250–260.
[16] Caporizzo, M. A., Chen, C. Y., Bedi, K., Margulies, K. B., and Prosser, B. L., Mar. 2020, "Microtubules Increase Diastolic Stiffness in Failing Human Cardiomyocytes and Myocardium," Circulation, 141(11), pp. 902–915.
[17] Tsutsui, H., Ishihara, K., and Cooper, G., IV, 1993, "Cytoskeletal Role in the Contractile Dysfunction of Hypertrophied Myocardium," Science, 260(5108), pp. 682–687.
[18] Tsutsui, H., Tagawa, H., Kent, R., McCollam, P., Ishihara, K., Nagatsu, M., and Cooper, G., IV, 1994, "Role of Microtubules in Contractile Dysfunction of Hypertrophied Cardiocytes," Circulation, 90(1), pp. 533–555.
[19] Liu, W., LeBar, K., Roth, K., Pang, J., Ayers, J., Chicco, A. J., Puttlitz, C. M., and Wang, Z., 2023, "Alterations of Biaxial Viscoelastic Properties of the Right Ventricle in Pulmonary Hypertension Development in Rest and Acute Stress Conditions," Front. Bioeng. Biotechnol., 11, p. 1182703.
[20] Avazmohammadi, R., Hill, M., Simon, M., and Sacks, M., 2017, "Transmural Remodeling of Right Ventricular Myocardium in Response to Pulmonary Arterial Hypertension," APL Bioeng, 1(1), p. 016105.
[21] Avazmohammadi, R., Hill, M. R., Simon, M. A., Zhang, W., and Sacks, M. S., 2017, "A Novel Constitutive Model for Passive Right Ventricular Myocardium: Evidence for Myofiber–Collagen Fiber Mechanical Coupling," Biomech. Model Mechanobiol., 16(2), pp. 561–581.
[22] Troyer, K. L., and Puttlitz, C. M., 2011, "Human Cervical Spine Ligaments Exhibit Fully Nonlinear Viscoelastic Behavior," Acta Biomater., 7(2), pp. 700–709.
[23] Troyer, K. L., Estep, D. J., and Puttlitz, C. M., 2012, "Viscoelastic Effects During Loading Play an Integral Role in Soft Tissue Mechanics," Acta Biomater., 8(1), pp. 234–243.
[24] Labus, K. M., and Puttlitz, C. M., 2016, "Viscoelasticity of Brain Corpus Callosum in Biaxial Tension," J. Mech. Phys. Solids, 96, pp. 591–604.
[25] Liu, W., Nguyen-Truong, M., LeBar, K., Labus, K. M., Gray, E., Ahern, M., Neelakantan, S., et al., 2022, "Multiscale Contrasts Between the Right and Left

Ventricle Biomechanics in Healthy Adult Sheep and Translational Implications," Front. Bioeng. Biotechnol., 10, p. 588.
[26] Wang, Z., Golob, M. J., and Chesler, N. C., 2016, "Viscoelastic Properties of Cardiovascular Tissues," Viscoelastic Viscoplast. Mater., 2, p. 64.
[27] Cox, R. H., 1984, "Viscoelastic Properties of Canine Pulmonary Arteries," Heart Circ. Physiol., 246(1), pp. 90–96.
[28] Xiao, H., Tan, I., Butlin, M., Li, D., and Avolio, A. P., 2017, "Arterial Viscoelasticity: Role in the Dependency of Pulse Wave Velocity on Heart Rate in Conduit Arteries," Heart Circ. Physiol., 312(6), pp. 1185–1194.
[29] Wang, Z., Lakes, R. S., Golob, M., Eickhoff, J. C., and Chesler, N. C., 2013, "Changes in Large Pulmonary Arterial Viscoelasticity in Chronic Pulmonary Hypertension," PLoS One, 8(11), p. e78569.
[30] Anssari-Benam, A., Tseng, Y.-T., Holzapfel, G. A., and Bucchi, A., 2019, "Rate-Dependency of the Mechanical Behaviour of Semilunar Heart Valves Under Biaxial Deformation," Acta Biomater., 88, pp. 120–130.
[31] Anssari-Benam, A., Tseng, Y.-T., Holzapfel, G. A., and Bucchi, A., 2020, "Rate-Dependent Mechanical Behaviour of Semilunar Valves Under Biaxial Deformation: From Quasi-Static to Physiological Loading Rates," J. Mech. Behav. Biomed. Mater., 104, p. 103645.
[32] Dokos, S., Smaill, B. H., Young, A. A., and LeGrice, I. J., 2002, "Shear Properties of Passive Ventricular Myocardium," Heart Circ. Physiol., 283(6), pp. 2650–2659.
[33] Humphrey, J. D., Strumpf, R. K., and Yin, F. C., 1990, "Biaxial Mechanical Behavior of Excised Ventricular Epicardium," Am. J. Physiol., 259(1), pp. 101–108.
[34] Cooper, G., 2000, "Cardiocyte Cytoskeleton in Hypertrophied Myocardium," Heart Failure Rev., 5(3), pp. 187–201.
[35] Nordsletten, D., Capilnasiu, A., Zhang, W., Wittgenstein, A., Hadjicharalambous, M., Sommer, G., Sinkus, R., and Holzapfel, G., 2021, "A Viscoelastic Model for Human Myocardium," Acta Biomater., 135, pp. 441–457.